

The Nature of the Interlayer Interaction in Bulk and Few-Layer Phosphorus

L. Shulenburger,¹ A.D. Baczewski,¹ Z. Zhu,² J. Guan,² and D. Tománek²

¹Sandia National Laboratories, Albuquerque NM 87185

²Michigan State University, East Lansing MI 48825

An outstanding challenge of theoretical electronic structure is the description of van der Waals (vdW) interactions in molecules and solids. Renewed interest in resolving this is in part motivated by the technological promise of layered systems including graphite, transition metal dichalcogenides, and more recently, black phosphorus, in which the interlayer interaction is widely believed to be dominated by these types of forces. We report a series of quantum Monte Carlo (QMC) calculations for bulk black phosphorus and related few-layer phosphorene, which elucidate the nature of the forces that bind these systems and provide benchmark data for the energetics of these systems. We find a significant charge redistribution due to the interaction between electrons on adjacent layers. Comparison to density functional theory (DFT) calculations indicate not only wide variability even among different vdW corrected functionals, but the failure of these functionals to capture the trend of reorganization predicted by QMC. The delicate interplay of steric and dispersive forces between layers indicate that few-layer phosphorene presents an unexpected challenge for the development of vdW corrected DFT.

There is growing interest in understanding and correctly describing the nature of the weak interlayer interaction in layered systems ranging from few-layer graphene¹ to transition metal dichalcogenides² such as MoS₂ and few-layer phosphorene^{3,4}, which display unique electronic properties and bear promise for device applications. Anticipating that challenges concerning the stability and isolation of single- to few-layer phosphorene can be overcome⁵, this system with its unique electronic^{3,4} and optical⁶ properties is attracting particular interest. It displays a high and anisotropic carrier mobility^{7,8} and a robust band gap that depends sensitively on the in-layer strain³. Progress in device fabrication^{4,9} indicates clearly that phosphorene holds technological promise. Since the fundamental band gap depends sensitively on the number of layers³, understanding the nature of the interlayer interaction is particularly important.

The standard approach to describe the interlayer interaction in layered solids has been based on DFT. Whereas DFT is – in principle – capable of describing the total energy of any system in the ground state exactly, current implementations describe the effects of electron exchange and correlation only in an approximate manner. In most covalent and ionic solids of interest, the specific treatment of exchange and correlation of electrons does not play a crucial role and commonly used local or semi-local exchange-correlation functionals of the electron density are adequate. This approach may, however, not be adequate in complex and weakly bonded systems¹⁰ including black phosphorus¹¹. This is illustrated in Fig. 1, which displays large differences between interlayer interaction energies in bulk and bilayer black phosphorus, obtained using different DFT functionals contained in the VASP software package^{12–14}. The large spread of the interlayer energies predicted using these functionals, some of which include van der Waals (vdW) corrections, illustrates the gravity of the issue.

Even though vdW corrected exchange-correlation functionals can improve the predicted geometry of lay-

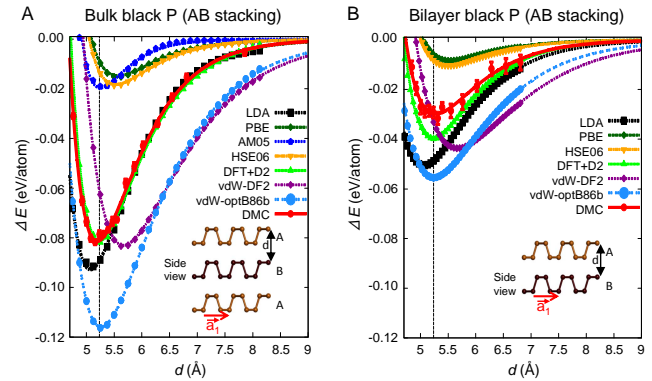


FIG. 1. Binding energy per atom ΔE as a function of the interlayer spacing d in AB stacked (A) bulk and (B) bilayer black phosphorus. QMC results obtained using diffusion Monte Carlo (DMC) are compared to DFT with LDA¹⁵, PBE¹⁶, AM05¹⁷, DFT+D2¹⁸, vdW-DF2¹⁹, vdW-optB86b^{20,21} and HSE06²² exchange-correlation functionals. The lines connecting the data points are Morse fits that extrapolate to $\Delta E = 0$ for $d \rightarrow \infty$. The vertical dashed line indicates the observed interlayer spacing d_e (expt.) = 5.2365 Å in the bulk structure in (A) and the optimum value based on DMC in the bilayer in (B). Side views of the geometries are shown in the insets.

ered phosphorus, other quantities such as the transition pressure from bulk orthorhombic to rhombohedral phases are significantly underestimated¹¹. This comes as no surprise, since recent benchmarks in dense hydrogen indicate that variations in the relative accuracy are observed among numerous vdW corrected functionals depending on the quantity being calculated²³. Even though the nature of the interactions in phosphorus is quite different from hydrogen, the difficulty to properly balance vdW and other interactions likely persists.

A superior way to obtain insight into the nature of the interlayer interaction requires a computational approach that treats electron exchange and correlation adequately

and on the same footing as covalent and ionic interactions. Unlike in DFT, where the fundamental quantity is the electron density, the fundamental quantity in QMC calculations is the properly antisymmetrized all-valence-electron wavefunction that explicitly describes the correlation of electrons. Therefore, the weak interlayer interaction in layered systems obtained using QMC is expected to be more precise than the DFT-based counterpart, and the electron density obtained by QMC likely provides a better representation of the true charge density than DFT. Should the QMC-based electron distribution in a few-layer system differ in a significant and nontrivial manner from a superposition of electron densities in isolated monolayers, we may surely conclude that the interlayer interaction in such a system is not purely dispersive in nature.

In the last decade, QMC methods have demonstrated considerable promise as a high accuracy first principles method for studying solids²⁴ and are especially well-suited to vdW bound systems²⁵⁻³¹. On one hand, the absence of approximations in treating the interaction between electrons makes it an ideal method for layered materials with a competition between different types of interactions. On the other hand, the computational cost associated QMC calculations is typically 1,000 – 10,000 times higher than that of comparable semilocal DFT calculations. Even though this cost is mitigated by its superior parallel scalability, QMC is – for the time being – most useful for benchmark calculations.

We have performed QMC calculations using the diffusion Monte Carlo (DMC) approach, as described in the Supplemental Material, in which details of the pseudopotential and an intensive procedure for converging finite size effects are included. One of the key approximations in our calculation is bias due to a fixed nodal surface. This was not anticipated to be significant in black phosphorus as the binding of interest occurs in a region of low electronic density for which the degree of nodal nonlinearity is expected to be low³². Nevertheless, some DMC calculations were carried out using orbitals from LDA, PBE, and vdW-optB86B functionals, to investigate the impact of the fixed node approximation. As the nodal surface associated with LDA orbitals were found to give the lowest energy and our method is variational, the LDA orbitals were subsequently used in all cases.

Our DMC results for the interlayer binding curves in bulk and bilayer black phosphorus are shown by the solid lines in Fig. 1. The total energy difference between the monolayer and the bulk system indicates that the binding energy of phosphorene sheets in black phosphorus is 81 ± 6 meV/atom, which translates to a cleavage energy of 22.4 ± 1.6 meV per \AA^2 of the interface area. This is larger than that for many other layered materials³³, but weak enough to allow mechanical exfoliation that has been reported.^{3,4}

Comparing the DMC results to a variety of different DFT functionals, significant variability is evident. Results are in agreement with intuition for LDA, PBE, and

HSE06 which do not treat vdW explicitly - namely that LDA overbinds and reduces the interlayer spacing in comparison to experiment, whereas GGA and HSE06 underbind. The gradient corrected AM05, designed to properly capture the energetics of the Airy gas at a jellium surface, has none of the spurious self-interaction in low density regions that cause LDA to overbind materials with vdW interactions. Nevertheless, it reproduces the bulk interlayer spacing correctly, but with only a quarter of the interlayer interaction energy predicted by DMC. That a vdW-free functional binds at all gives some indication that the character of the interlayer interaction in these systems is not strictly vdW.

From the wide array of available vdW functionals, we have selected 3 exemplary of increasing levels of sophistication. DFT+D2 is based upon an empirical correction to the total energy in the form of a simple pair-wise interaction parameterized by atomic C_6 coefficients. vdW-optB86b and vdW-DF2 are more advanced, both based upon improvements to the non-local vdW-DF functional³⁴. Significant variability is evident in both energetics and the equilibrium interlayer spacing among these functionals. It is interesting to note that the least sophisticated of these functionals (DFT+D2) performs the best relative to DMC, as well as experiment in the case of the bulk system.

Contrasting the bulk and bilayer binding curves, it is evident that DMC predicts that the interlayer interaction is not strictly additive. For an additive interaction, we should expect that the binding energy of the bilayer would be approximately 1/2 that of the bulk system because both layers are missing half of their neighboring layers. Instead, DMC predicts that this is not the case and that the bilayer binding energy is instead 3/8 that of the bulk system. The results for vdW corrected DFT (DFT+D2, vdW-opB86b, and vdW-DF2) are more indicative of an additive interlayer interaction, giving us another indication that the nature of the interlayer binding in black phosphorus is richer than a simple vdW interaction.

A more direct indication of the character of the interlayer binding is the charge density difference induced by assembling the bulk system from isolated monolayers. We computed the quantity $\Delta\rho = \rho_{tot}(bulk) - \sum \rho_{tot}(monolayers)$ using both DMC and DFT to investigate this. The l_1 -norm of $\Delta\rho$ over the unit cell is an indicator of the number of electrons being redistributed due to interlayer interaction. In all DFT functionals considered in this study, this metric indicates a motion of fewer than 0.03 electrons per atom. In contrast, it predicts a motion of 0.15 electrons per atom in DMC. To provide insight into the nature of this significant redistribution, the density difference is visualized in Fig. 2A. Inspection indicates that charge is pushed out of the region between layers and into the covalent bonds within each layer. This picture is well supported by basic chemical intuition. In an isolated layer, each atom is 3-fold coordinated with sp^3 bonding character and a single lone

pair protruding away from the layer. Bringing layers together will increase the overlap between these lone pairs on adjacent layers and steric forces will tend to drive the affiliated lone pair charge closer to the layer on which it originated.

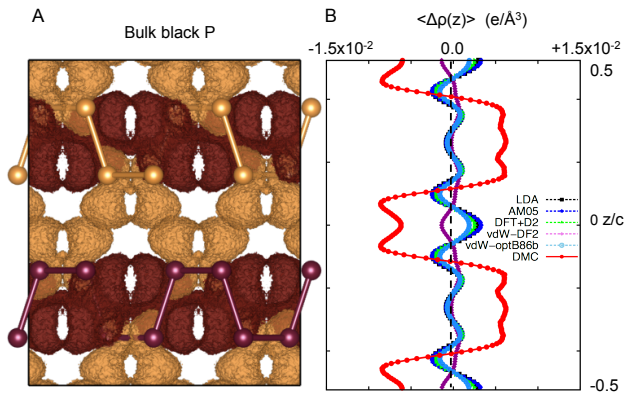


FIG. 2. Electron density difference $\Delta\rho = \rho_{tot}(bulk) - \sum \rho_{tot}(monolayers)$ representing the charge redistribution caused by assembling the bulk structure from isolated monolayers. (A) DMC isosurfaces bounding regions of excess electron density (dark brown) and electron deficiency (light brown), with respective values $\pm 6.5 \times 10^{-3} e/\text{\AA}^3$. (B) $\langle \Delta\rho(z) \rangle$ for DMC and several DFT functionals averaged across the $x - y$ plane of the layers, with z/c indicating the relative position of the plane in the unit cell.

To further elucidate the role that this charge redistribution plays in the interlayer binding, the planar average of the charge density difference along planes perpendicular to the interlayer axis for both DMC and several DFT functionals are illustrated in Fig. 2B. It remains evident that DMC predicts an average depletion of charge between layers and commensurate accumulation in-layer. However, with the exception of vdW-DF2, this trend is not evident in any of the DFT calculations. Instead, DFT predicts a weak accumulation of charge between layers, indicating a minor covalent character in addition to whatever vdW binding is present. This likely explains why a vdW-free functional like AM05 weakly binds the system near the correct interlayer spacing. The case of vdW-DF2 is of particular interest because it is the only functional that predicts a qualitatively similar, but considerably weaker, trend as DMC. Among DFT+D2, vdW-optB86b, and vdW-DF2, vdW-DF2 is the most theoretically sophisticated so that it gets closer to the trend predicted by DMC is unsurprising. Even so, that DFT+D2 gives the best performance in terms of energetics and geometry indicates that this functional may be getting the right answer for reasons that are not necessarily consistent with the many-body physics more explicitly explored through DMC.

Recent work on self-consistent vdW functionals indicate that the charge redistribution induced by vdW interactions can play an important role in the energetics of highly polarizable systems³⁵. In this work, the authors

note that this subtle physics is consistent with an early observation by Feynman³⁶ in which the vdW interaction can be viewed as arising from an attractive interaction induced through a small accumulation of charge density between two mutually perturbed neutral systems. In the case of black phosphorus, we find that this picture of the vdW interaction is balanced by the steric redistribution of charge away from the region between layers. Based upon the results elucidated by our DMC calculations, we anticipate that getting this balance right may be a critical requirement to examine in developing more advanced DFT functionals for layered compounds.

The corresponding difference between the charge density in an isolated monolayer and within a layer of bulk phosphorus is likely to affect the in-plane bonding and geometry. To see if this is indeed the case, we have calculated the energy change ΔE as a function of a stretch applied along the softer axis \bar{a}_1 of the sheets. Our results for the bulk system, presented in Fig. 3, indicate an excellent agreement (to within half a percent) between the optimized lattice constant $a_1(\text{theory}) = 4.404 \pm 0.019 \text{ \AA}$ and the observed value³⁷ $a_1(\text{expt.}) = 4.374 \text{ \AA}$ in the bulk structure. Further, we can see precisely how soft this axis is in both systems, with a deformation by $|\Delta a_1| \lesssim 0.3 \text{ \AA}$ requiring an energy investment of only $\approx 5 \text{ meV/atom}$ in a monolayer or in bulk black phosphorus. This energy corresponds to a thermal energy of 60 K, and we should expect significant thermal fluctuations of the geometry of unsupported phosphorene sheets at ambient temperature and pressure. Most important, however, is the comparison between a_1 in the isolated monolayer and in the bulk structure. Our DMC results indicate a change in the in-plane stiffness along the soft axis and an $\approx 2\%$ reduction in the equilibrium lattice constant a_1 in a monolayer from the bulk value. This is another indication of a charge redistribution during the formation of a layered bulk structure from monolayers that modifies the covalent interaction within the layers. This again supports our finding that the interlayer interaction in black phosphorus is not purely dispersive.

To gain additional insight into the nature of the interlayer interaction, we compare in Fig. 4 the bonding within an AA and AB stacked bilayer as a function of the interlayer separation d . Our DMC results in Fig. 4 indicate that the AB stacking, which occurs in the bulk material, persists also in the bilayer.

The cleavage energy of an AB stacked bilayer is $16.6 \pm 2.2 \text{ meV/\AA}^2$, thus 26% smaller than the bulk cleavage energy of $22.4 \pm 1.6 \text{ meV/\AA}^2$. The exfoliation energy associated with removing the topmost layer from the surface is expected to lie between these two values. The findings appear plausible also in view of the fact that in graphite, the cleavage energy is estimated to be 18% larger than the exfoliation energy³⁸. Though we expect the interlayer interaction to be mediated primarily by the π electrons in graphite and sp^3 -like lone pairs with a different character in black phosphorus, the ratio of the exfoliation and cleavage energy in the two systems

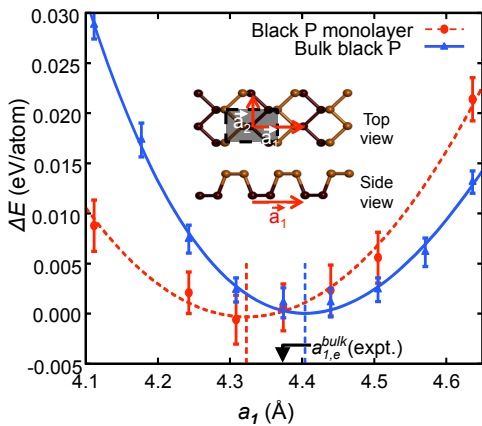


FIG. 3. DMC results for the relative total energy per atom ΔE as a function of the in-layer lattice constant a_1 in the soft direction of a phosphorene monolayer and of bulk black phosphorus. The lines connecting the data points are Morse fits that extrapolate to $\Delta E = 0$ for $d \rightarrow \infty$. The optimum lattice constant values for both structures are indicated by the vertical dashed lines. The observed value $a_{1,e}^{\text{bulk}}(\text{expt.}) = 4.374 \text{ \AA}$ in the bulk structure is indicated by the arrow. The monolayer geometry is shown in the inset.

appears to be similar.

The interlayer spacing $d_e = 5.272 \pm 0.023 \text{ \AA}$ in the AB-stacked bilayer is about 1% larger than our calculated value for the bulk material. In the less favorable AA stacking geometry, the binding energy is three times smaller than in the AB geometry, which should effectively prevent formation of stacking faults, at least in the absence of impurities. The significant difference between the interaction in the AA and AB stacked bilayer suggests that the interaction between the sheets is more complicated than the vdW interaction between two homogeneous slabs. Were the interlayer interaction purely dispersive, the registry of layers would not matter much and the AA and AB binding energies as well as interlayer separations should be nearly identical.

To shed some light on the sensitivity of the interlayer bonding on the stacking sequence, we investigated the change in the charge density $\Delta\rho$ induced by the interaction. Our results for AB and AA stackings are shown in Fig. 4C. Similar to the corresponding results for bulk black phosphorus in Fig. 2B, the $\Delta\rho$ plots for the bilayer show a significant rearrangement of the electronic charge, a total of ≈ 0.075 electrons per atom in both cases. In the AB-stacked bilayer, similar to the bulk system, we observe a depletion of the electron density in the region between the sheets and electron accumulation within the layers. The charge redistribution in the AA bilayer is significantly different, even including small regions in the interlayer space where the charge density increases. The large difference between $\Delta\rho$ in the AA and AB stacked bilayer is inconsistent with purely dispersive bonding and explains why the interlayer spacing and binding energy are so different in the two systems.

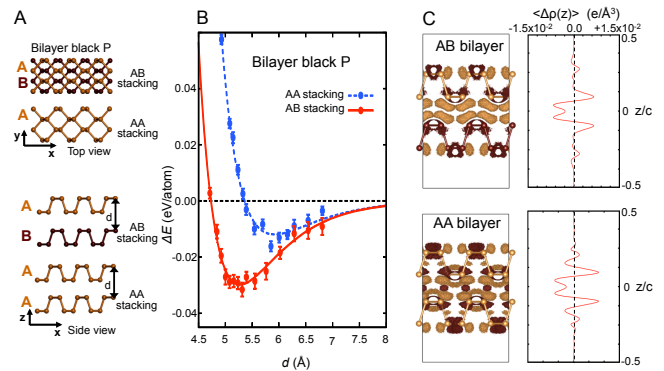


FIG. 4. DMC results for bonding in AA and AB stacked phosphorene bilayers. (A) Geometry of an AA and AB stacked bilayer in top and side view. (B) DMC results for the relative total energy per atom ΔE as a function of the interlayer spacing d . The lines connecting the data points are Morse fits that extrapolate to $\Delta E = 0$ for $d \rightarrow \infty$. (C) Electron density differences for the AB and AA bilayers illustrated using isosurfaces and planar averaging as in Fig. 3 (with the same color coding).

In summary, we studied the nature of the interlayer interaction in layered black phosphorus using quantum Monte Carlo calculations, which describe the correlation of electrons explicitly by an antisymmetrized all-valence-electron wavefunction and treat covalent and dispersive interactions on the same footing. Unlike in true vdW systems, we find that the interlayer interaction in few-layer phosphorene is associated with a significant charge redistribution between the in-layer and interlayer region, caused by changes in the non-local correlation of electrons in adjacent layers. Consequently, the resulting interlayer interaction can not be described properly by density functional theory (DFT) augmented by mere semi-local vdW correction terms, and thus the designation ‘van der Waals solids’ is improper for systems including few-layer phosphorene. Our results may be used as benchmarks for developing more sophisticated DFT functionals that should provide an improved description of non-local electron correlations in layered systems.

We are grateful for useful comments and conversations with Paul Kent, Jeongnim Kim, Ann Mattsson, Jonathan Moussa, Lydia Nemeč, and Gotthard Seifert. Calculations were performed on *Sequoia* at Lawrence Livermore National Laboratory and *Mira* at the Argonne Leadership Computing Facility. We thank Anouar Benali for assistance performing calculations on *Mira*. An award of computer time was provided by the Innovative and Novel Computational Impact on Theory and Experiment (INCITE) program with Project CPH103. A.B. and L.S. were supported through the Predictive Theory and Modeling for Materials and Chemical Science program by the Office of Basic Energy Sciences (BES), Department of Energy (DOE). Z.Z., J.G., and D.T. acknowledge support by the National Science Foundation Cooperative Agreement No. EEC-0832785, title “NSEC: Center for

High-Rate Nanomanufacturing”. Sandia National Laboratories is a multi-program laboratory managed and operated by Sandia Corporation, a wholly owned subsidiary

of Lockheed Martin Corporation, for the U.S. Department of Energy’s National Nuclear Security Administration under contract DE-AC04-94AL85000.

-
- ¹ K. S. Novoselov, D. Jiang, F. Schedin, T. J. Booth, V. V. Khotkevich, S. Morozov, and A. Geim, *Proc. Natl. Acad. Sci. (USA)* **102**, 10451 (2005).
 - ² H. L. Zhuang and R. G. Hennig, *J. Phys. Chem. C* **117**, 20440 (2013).
 - ³ H. Liu, A. T. Neal, Z. Zhu, Z. Luo, X. Xu, D. Tománek, and P. D. Ye, *ACS Nano* **8**, 4033 (2014).
 - ⁴ L. Li, Y. Yu, G. J. Ye, Q. Ge, X. Ou, H. Wu, D. Feng, X. H. Chen, and Y. Zhang, *Nature Nano.* **9**, 372 (2014).
 - ⁵ A. Castellanos-Gomez, L. Vicarelli, E. Prada, J. O. Island, K. L. Narasimha-Acharya, S. I. Blanter, D. J. Groenendijk, M. Buscema, G. A. Steele, J. V. Alvarez, H. W. Zandbergen, J. J. Palacios, and H. S. J. van der Zant, *2D Materials* **1**, 025001 (2014).
 - ⁶ V. Tran, R. Soklaski, Y. Liang, and L. Yang, *Phys. Rev. B* **89**, 235319 (2014).
 - ⁷ N. Gillgren, D. Wickramaratne, Y. Shi, T. Espiritu, J. Yang, J. Hu, J. Wei, X. Liu, Z. Mao, K. Watanabe, T. Taniguchi, M. Bockrath, Y. Barlas, R. K. Lake, and C. N. Lau, *2D Mater.* **2**, 011001 (2015).
 - ⁸ R. Fei and L. Yang, *Nano Lett.* **14**, 2884 (2014).
 - ⁹ S. P. Koenig, R. A. Doganov, H. Schmidt, A. H. Castro Neto, and B. Özyilmaz, *Appl. Phys. Lett.* **104**, 103106 (2014).
 - ¹⁰ G. Cicero, J. C. Grossman, E. Schwegler, F. Gygi, and G. Galli, *J. Am. Chem. Soc.* **130**, 1871 (2008).
 - ¹¹ S. Appalakondaiah, G. Vaitheeswaran, S. Lebègue, N. E. Christensen, and A. Svane, *Phys. Rev. B* **86**, 035105 (2012).
 - ¹² G. Kresse and J. Furthmüller, *Phys. Rev. B* **54**, 11169 (1996).
 - ¹³ G. Kresse and J. Furthmüller, *Comp. Mat. Sci.* **6**, 15 (1996).
 - ¹⁴ G. Kresse and D. Joubert, *Phys. Rev. B* **59**, 1758 (1999).
 - ¹⁵ J. P. Perdew and A. Zunger, *Phys. Rev. B* **23**, 5048 (1981).
 - ¹⁶ J. P. Perdew, K. Burke, and M. Ernzerhof, *Phys. Rev. Lett.* **77**, 3865 (1996).
 - ¹⁷ R. Armiento and A. E. Mattsson, *Phys. Rev. B* **72**, 085108 (2005).
 - ¹⁸ S. Grimme, *J. Comput. Chem.* **27**, 1787 (2006).
 - ¹⁹ K. Lee, E. D. Murray, L. Kong, B. I. Lundqvist, and D. C. Langreth, *Phys. Rev. B* **82**, 081101 (2010).
 - ²⁰ J. Klimeš, D. R. Bowler, and A. Michaelides, *J. Phys.: Cond. Matt.* **22**, 022201 (2010).
 - ²¹ J. Klimeš, D. R. Bowler, and A. Michaelides, *Phys. Rev. B* **83**, 195131 (2011).
 - ²² A. V. Krukau, O. A. Vydrov, A. F. Izmaylov, and G. E. Scuseria, *J. Chem. Phys.* **125**, 224106 (2006).
 - ²³ R. C. Clay, J. Mcminis, J. M. McMahon, C. Pierleoni, D. M. Ceperley, and M. A. Morales, *Phys. Rev. B* **89**, 184106 (2014).
 - ²⁴ L. Shulenburger and T. R. Mattsson, *Phys. Rev. B* **88**, 245117 (2013).
 - ²⁵ N. D. Drummond and R. J. Needs, *Phys. Rev. B* **73**, 024107 (2006).
 - ²⁶ S. Sorella, M. Casula, and D. Rocca, *J. Chem. Phys.* **127**, 014105 (2007).
 - ²⁷ L. Spanu, S. Sorella, and G. Galli, *Phys. Rev. Lett.* **103**, 196401 (2009).
 - ²⁸ A. Benali, L. Shulenburger, N. A. Romero, J. Kim, and O. A. von Lilienfeld, *J. Chem. Theory Comput.* **10**, 3417 (2014).
 - ²⁹ P. Ganesh, J. Kim, C. Park, M. Yoon, F. A. Reboredo, and P. R. C. Kent, *J. Chem. Theory Comput.* **10**, 5318 (2014).
 - ³⁰ M. Dubecký, P. Jurečka, R. Derian, P. Hobza, M. Otyepka, and L. Mitas, *J. Chem. Theory Comput.* **9**, 4287 (2013).
 - ³¹ M. Dubecký, R. Derian, P. Jurečka, L. Mitas, P. Hobza, and M. Otyepka, *Phys. Chem. Chem. Phys.* **16**, 20915 (2014).
 - ³² K. M. Rasch, S. Hu, and L. Mitas, *The Journal of chemical physics* **140**, 041102 (2014).
 - ³³ T. Björkman, A. Gulans, A. V. Krasheninnikov, and R. M. Nieminen, *Phys. Rev. Lett.* **108**, 235502 (2012).
 - ³⁴ M. Dion, H. Rydberg, E. Schröder, D. C. Langreth, and B. I. Lundqvist, *Phys. Rev. Lett.* **92**, 246401 (2004).
 - ³⁵ N. Ferri, R. A. DiStasio Jr, A. Ambrosetti, R. Car, and A. Tkatchenko, *Phys. Rev. Lett.* **114**, 176802 (2015).
 - ³⁶ R. P. Feynman, *Phys. Rev.* **56**, 340 (1939).
 - ³⁷ L. Cartz, S. R. Srinivasa, R. J. Riedner, J. D. Jorgensen, and T. G. Worlton, *J. Chem. Phys.* **71**, 1718 (1979).
 - ³⁸ L. Girifalco and R. Lad, *J. Chem. Phys.* **25**, 693 (1956).

Supplemental Materials for: The Nature of the Interlayer Interaction in Bulk and Few-Layer Phosphorus

I. CONVERGENCE OF FINITE-SIZE EFFECTS

One- and two-body finite size effects must be considered in both the bulk and planar periodic structures. One-body effects are corrected using canonical twist averaging^{S6}, while two-body effects are extrapolated. Controlling the two-body effects present a challenge for extrapolation consistent with reports of calculations done on graphite.^{S7}

For the bulk systems, we consider two types of tilings for generating these supercells. We expect finite size effects to converge more quickly when increasing the effective system size along the layering axis rather than in-plane. Consequently, we study two-body effects for 2x2x1, 3x3x1, 4x4x1, and 5x5x1 tilings (single layer) and 2x2x2, 3x3x2, and 4x4x2 (bilayer) in the bulk.

However, the peculiar nature of the electron correlation in two dimensional systems such as black phosphorus coupled with the meV accuracy required for this study requires a slightly different procedure for assessing and reducing the two body finite size effects introduced by simulating a supercell with periodic boundary conditions. The typically used procedures for this involve either utilizing a model interaction that removes spurious electron correlation,^{S8} analyzing the behavior of the structure factor and two body jastrow factor for small values or momentum transfer^{S9} or utilizing calculations with density functionals designed to mimic the energetics of the electron correlation in finite supercells.^{S10} As generally practiced, all of these procedures rely on the assumption that the electron correlation is isotropic, a condition that is grossly violated in a layered material like black phosphorus.

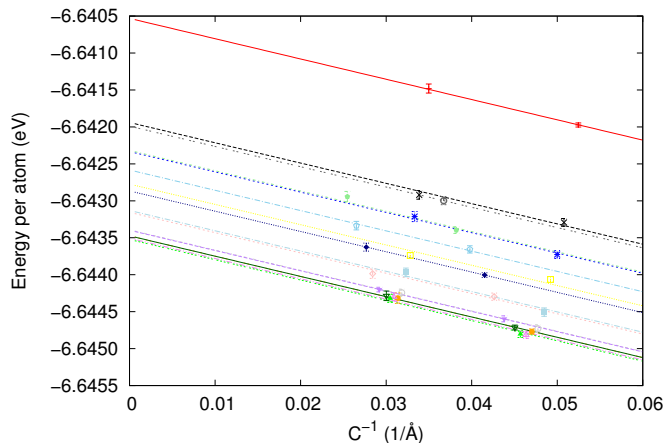


FIG. S1. Energy per atom of black phosphorus as a function of the inverse of the shortest distance between periodic images of phosphorene sheets. The identical slope of the lines enforces consistency in the extrapolation for calculations where the distance between adjacent sheets are varied.

This difficulty has been noted in previous quantum Monte Carlo studies of layered materials^{S7} where a combination of the KZK functional^{S10} was used for correlations in the plane and an extrapolation scheme was used for correlations in the direction perpendicular to the planes. Our approach is to extend this methodology in two regards. Firstly, we utilize extrapolation in the size of the supercell to determine correlations both in plane and out of plane and secondly, because such extrapolations can introduce a significant amount of noise in the extrapolated quantities, we correlate the parameters of the extrapolations between systems with similar geometries. This is best illustrated looking at the extrapolation of the energy in the direction perpendicular to the phosphorene planes.

This correlation may be expected to decrease with distance between the planes and also be a function of the number of layers simulated. To capture this, we extrapolate based on the total distance between images in the perpendicular direction and also require that the slope of the extrapolation be a simple function of the distance between the planes. The results of this procedure are shown in fig S1, where the energy per atom for different supercells with different spacings between the phosphorene planes and different numbers of layers in the supercell are shown as a function of the inverse of the distance between the top and bottom of the supercell. All of these calculations had a three by three tiling of the primitive cell of phosphorus in the direction parallel to the planes and both the spacing between the layers and the number of copies of the supercell were varied. A similar procedure was used to extrapolate to infinite size supercells in the other direction.

II. NUMERICAL CONSIDERATIONS

To control computational cost, we verify that our choice of DMC time step satisfies a balance between efficient sampling and having a large time step bias. In doing so, for each system we choose fixed moderately sized supercells and perform short DMC runs at different time steps. A best fit line is constructed for the energy as a function of time step and we choose to use the largest time step that is within 1 mHa/atom of the zero time step extrapolated energy. We have found that a time step of 0.0075 a.u. is adequate to achieve this level of accuracy in all cases.

Further, to control the memory required by the wave function we assess the effect of enlarging the grid spacing associated with the B-spline representation of the Kohn-Sham orbitals relative to the equivalent real space grid used in the plane wave pseudopotential calculation in which they are generated. The convergence of the total energy, kinetic energy, and variance in the local energy are assessed in determining the appropriate grid spacing. Noting that the variance converges most slowly in the grid spacing, an enlargement factor of 4/3 preserves accuracy while reducing the memory used up in representing the wave function.

III. PSEUDOPOTENTIAL GENERATION AND TESTING

Two different pseudopotentials were generated for this study, one treating 5 valence electrons and the other treating 13. Both pseudopotentials were generated using the opium pseudopotential generation code.^{S1} The benchmark quantities under consideration are the equilibrium properties of a phosphorus dimer and the ionization potential and electron affinity of an isolated phosphorus atom.

In Table I some atomic benchmarks are given. While the accuracy relative to experiment is comparable for the ionization potential for both pseudopotentials, the 5 electron pseudopotential performs worse for the electron affinity. Given the relatively primitive trial wavefunction used, these results should not be taken as conclusive, but errors due to the nodal surface are generally less than a few tenths of an eV.

	5 electron	13 electron	Experiment
Ionization Potential	10.7112 ± 0.00084	10.6832 ± 0.0598	10.48669
Electron Affinity	0.6405 ± 0.0084	0.7483 ± 0.0626	0.746609

TABLE I. Ionization potential and electron affinity of an isolated phosphorus atom computed using two different pseudopotentials.

We also calculate the binding energy, atomization energy and vibrational frequency for the phosphorus dimer by calculating the energy as a function of bond length. The results of these calculations for each pseudopotential and a fit to a morse potential are shown in Figure S2 and the resulting observables are summarized in Table II.

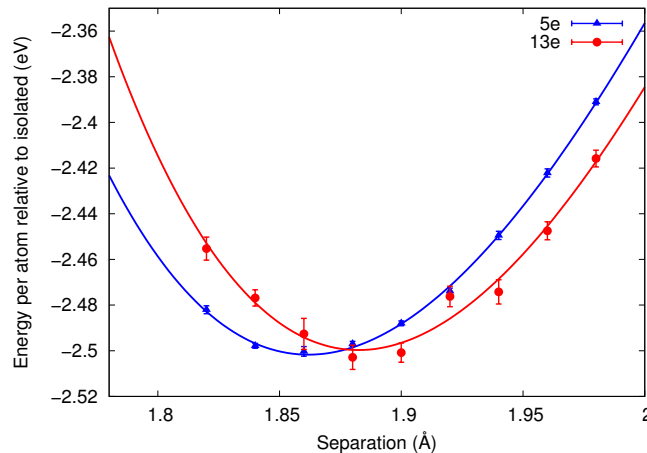


FIG. S2. Phosphorus dimer energy vs bond length curves for 5 and 13 electron pseudopotentials. Experimental values for the ionization potential and electron affinity are taken from References S2 and S3 respectively.

	5 electron	13 electron	Experiment
bond length (Å)	1.8618 ± 0.009	1.8824 ± 0.0018	1.89340 ± 0.00044
vibrational frequency (cm^{-1})	827.3 ± 9.4	851.7 ± 31.8	780.77
atomization energy (eV)	4.900 ± 0.001	4.894 ± 0.040	5.03 ± 0.02

TABLE II. Properties of phosphorus dimer computed using two different pseudopotentials. The experimental bond length, vibrational frequency and atomization energy are taken from references S4, S5 and S4 respectively.

While both the 5 electron and 13 electron pseudopotentials have similar accuracy relative to experiment, calculations using the potential with 13 electrons in the valence are nearly 100 times more expensive than those using the 5 electron potential. Therefore, its success in these metrics leads us to use the 5 electron pseudopotential for all remaining calculations on bulk phosphorus and phosphorene.

-
- [S1] *Opium pseudopotential package*, URL <http://opium.sourceforge.net>.
- [S2] R. J. Peláez, C. Blondel, M. Vandevraye, C. Drag, and C. Delsart, *Journal of Physics B: Atomic, Molecular and Optical Physics* **44**, 195009 (2011).
- [S3] N. Svendenius, *Physica Scripta* **22**, 240 (1980).
- [S4] K.-P. Huber and G. Herzberg, *Constants of diatomic molecules* (Springer, 1979).
- [S5] K. K. Irikura, *Journal of Physical and Chemical Reference Data* **36** (2007).
- [S6] C. Lin, F. Zong, and D. Ceperley, *Phys. Rev. E* **64**, 016702 (2001).
- [S7] L. Spanu, S. Sorella, and G. Galli, *Phys. Rev. Lett.* **103**, 196401 (2009).
- [S8] L. M. Fraser, W. M. C. Foulkes, G. Rajagopal, R. J. Needs, S. D. Kenny, and A. J. Williamson, *Phys. Rev. B* **53**, 1814 (1996).
- [S9] S. Chiesa, D. M. Ceperley, R. M. Martin, and M. Holzmann, *Phys. Rev. Lett.* **97**, 076404 (2006).
- [S10] H. Kwee, S. Zhang, and H. Krakauer, *Phys. Rev. Lett.* **100**, 126404 (2008).